

DTIC FILE COPY

REPORT SSD-TR-90-38

4

**AD-A229 360**

## **Reactive Removal of BiF Ground State**

**Prepared by**

**J. S. HOLLOWAY and J. B. KOFFEND  
Aerophysics Laboratory  
Laboratory Operations  
The Aerospace Corporation  
El Segundo, CA 90245-4691**

**28 September 1990**

**Prepared for**

**SPACE SYSTEMS DIVISION  
AIR FORCE SYSTEMS COMMAND  
Los Angeles Air Force Base  
P.O. Box 92960  
Los Angeles, CA 90009-2960**

**APPROVED FOR PUBLIC RELEASE;  
DISTRIBUTION UNLIMITED**

**DTIC  
ELECTE  
NOV 28 1990  
S B D**

**00 11 27 043**

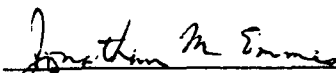
This report was submitted by The Aerospace Corporation, El Segundo, CA 90245, under Contract No. F04701-88-C-0089 with the Space Systems Division, P. O. Box 92960, Los Angeles, CA 90009-2960. It was reviewed and approved for The Aerospace Corporation by R. W. Fillers, Director, Aerophysics Laboratory. Capt R. Riviere was the project officer for the Mission-Oriented Investigation and Experimentation (MOIE) Program.

This report has been reviewed by the Public Affairs Office (PAS) and is releasable to the National Technical Information Service (NTIS). At NTIS, it will be available to the general public, including foreign nationals.

This technical report has been reviewed and is approved for publication. Publication of this report does not constitute Air Force approval of the report's findings or conclusions. It is published only for the exchange and stimulation of ideas.



RAFAEL A. RIVIERE, Capt, USAF  
MOIE Project Officer  
SSD/CNL



JONATHAN M. EMMES, Maj, USAF  
MOIE Project Manager  
AFSTC/WCO OL-AB

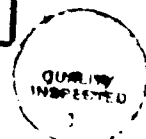
# REPORT DOCUMENTATION PAGE

1a. REPORT SECURITY CLASSIFICATION Unclassified			1b. RESTRICTIVE MARKINGS	
2a. SECURITY CLASSIFICATION AUTHORITY			3. DISTRIBUTION/AVAILABILITY OF REPORT Approved for pubic release; distribution unlimited	
2b. DECLASSIFICATION/DOWNGRADING SCHEDULE				
4. PERFORMING ORGANIZATION REPORT NUMBER(S) TR-0090(5930-04)-1			5. MONITORING ORGANIZATION REPORT NUMBER(S) SSD-TR-90-38	
6a. NAME OF PERFORMING ORGANIZATION The Aerospace Corporation Laboratory Operations		6b. OFFICE SYMBOL (If applicable)	7a. NAME OF MONITORING ORGANIZATION Space Systems Division	
6c. ADDRESS (City, State, and ZIP Code) El Segundo, CA 90245-4691			7b. ADDRESS (City, State, and ZIP Code) Los Angeles Air Force Base Los Angeles, CA 90009-2960	
8a. NAME OF FUNDING/SPONSORING ORGANIZATION		8b. OFFICE SYMBOL (If applicable)	9. PROCUREMENT INSTRUMENT IDENTIFICATION NUMBER F04701-88-C-0089	
8c. ADDRESS (City, State, and ZIP Code)			10. SOURCE OF FUNDING NUMBERS	
			PROGRAM ELEMENT NO.	PROJECT NO.
			TASK NO.	WORK UNIT ACCESSION NO.
11. TITLE (Include Security Classification) Reactive Removal of BiF Ground State				
12. PERSONAL AUTHOR(S) Holloway, John S. and Koffend, John B.				
13a. TYPE OF REPORT		13b. TIME COVERED FROM _____ TO _____		14. DATE OF REPORT (Year, Month, Day) 1990 September 28
				15. PAGE COUNT 26
16. SUPPLEMENTARY NOTATION				
17. COSATI CODES			18. SUBJECT TERMS (Continue on reverse if necessary and identify by block number)	
FIELD	GROUP	SUB-GROUP	Broida oven Photolysis	
19. ABSTRACT (Continue on reverse if necessary and identify by block number)				
<p>The reactivity of the ground state of bismuth monofluoride, <math>\text{BiF}(\text{XO}^+)</math>, has been investigated with a number of fluorine atom donors at several different temperatures. The measurements have been accomplished both by means of a time resolved, photolytically initiated experiment and on steady-state densities in a flow tube reactor. Both methods provide consistent results. The rate coefficients obtained span a range of over 3 orders of magnitude: <math>\text{F}_2</math> is found to be fairly efficient (<math>2.0 \times 10^{-11} \text{ cm}^3/\text{molecule-sec}</math>), while the series of nitrogen fluorides <math>\text{NF}_2</math>, <math>\text{NF}_3</math>, <math>\text{N}_2\text{F}_4</math> is quite inert (<math>6.2</math>, <math>5.0</math>, <math>7.8 \times 10^{-15} \text{ cm}^3/\text{molecule-sec}</math>, respectively). We observe <math>\text{BiF}(\text{XO}^+)</math> formation with a rate coefficient of <math>8.1 \times 10^{-12} \text{ cm}^3/\text{molecule-sec}</math> from <math>\text{NF}_2 + \text{Bi}</math> following the photolysis of <math>\text{Bi}(\text{CH}_3)_3</math> at 193 nm. We are also able to estimate a formation constant for <math>\text{Bi} + \text{F}_2</math> of about <math>1 \times 10^{-9} \text{ cm}^3/\text{molecule-sec}</math>. The stability of <math>\text{Bi}(\text{CH}_3)_3</math> with <math>\text{NF}_2</math> is discussed.</p>				
20. DISTRIBUTION/AVAILABILITY OF ABSTRACT <input checked="" type="checkbox"/> UNCLASSIFIED/UNLIMITED <input type="checkbox"/> SAME AS RPT. <input type="checkbox"/> DTIC USERS			21. ABSTRACT SECURITY CLASSIFICATION Unclassified	
22a. NAME OF RESPONSIBLE INDIVIDUAL			22b. TELEPHONE (Include Area Code)	22c. OFFICE SYMBOL

## PREFACE

This work was supported by the Air Force Weapons Laboratory under Air Force Space Systems Division Contract No. F04701-88-C-0089.

Accession For	
NTIS GRA&I	<input checked="checked" type="checkbox"/>
DTIC TAB	<input type="checkbox"/>
Unannounced	<input type="checkbox"/>
Justification	
By	
Distribution/	
Availability Codes	
Dist	Avail and/or Special
A-1	



## CONTENTS

I.	INTRODUCTION .....	5
II.	EXPERIMENTAL .....	7
III.	RESULTS AND DISCUSSION .....	11
	A. Flow Tube Kinetic Measurements .....	11
	B. Photo-Initiated Kinetics .....	16
IV.	CONCLUSION .....	23
	REFERENCES .....	25

## FIGURES

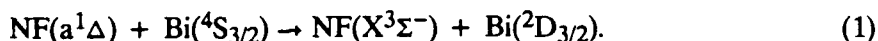
1.	Diagram of the Experimental Apparatus .....	8
2.	BiF A-X Laser-Induced Fluorescence Intensity Plotted as a Function of Reactant Density .....	13
3.	Time Resolved BiF A-X Laser-Induced Fluorescence from the 193 nm Photolysis of a Mixture of $F_2$ ( $1.37 \times 10^{14}$ molecules/cm <sup>3</sup> ), Ar ( $1.87 \times 10^{17}$ atoms/cm <sup>3</sup> ), $SF_6$ ( $7.55 \times 10^{16}$ molecules/cm <sup>3</sup> ), and $Bi(CH_3)_3$ ( $7.76 \times 10^{12}$ molecules/cm <sup>3</sup> ) at 25°C .....	17
4.	Plot of BiF A-X Laser-Induced Fluorescence Decay Rates from the 193 nm Photolysis of $F_2$ /Ar/ $SF_6$ / $Bi(CH_3)_3$ Mixtures at 25°C .....	17
5.	Plots of BiF A-X Laser-Induced Fluorescence Decay and Rise Rates from ArF Laser Initiation of $NF_2$ /Ar/ $SF_6$ / $Bi(CH_3)_3$ Mixtures at 198°C .....	19
6.	Plot of $Bi(CH_3)_3$ Single Exponential Removal Rates by its Reaction with $NF_2$ at 205°C .....	22

## TABLES

1.	Results of $BiF + X$ .....	14
2.	Bismuth and Nitrogen Fluoride Bond Dissociation Energies .....	15

## I. INTRODUCTION

This laboratory's acquaintance with the bismuth monofluoride molecule began with the observation of its blue  $\text{AO}^+ \rightarrow \text{XO}^+$  emission system during the course of flow tube studies.<sup>1</sup> The object of that research<sup>2</sup> was to scale the density of excited bismuth atoms based on resonant energy transfer from  $\text{NF}(a^1\Delta)$ :



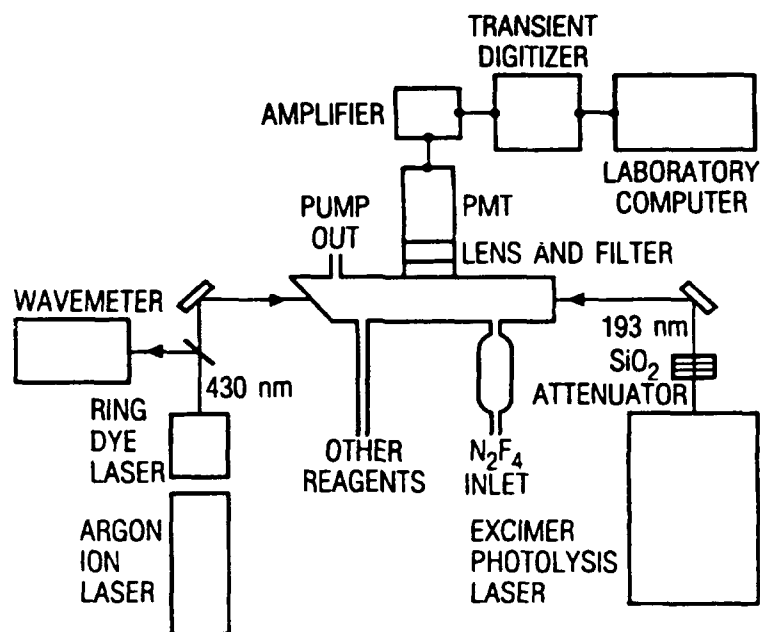
Instead of achieving the anticipated increase in  $\text{Bi}(^2\text{D})$  as  $\text{NF}(a)$  densities were raised, the experiment resulted in the generation of significant amounts of electronically excited  $\text{BiF}(\text{AO}^+)$ . Its visible band system,<sup>3</sup> 1.4  $\mu\text{sec}$  radiative lifetime,<sup>4</sup> and the apparent efficiency of its production are attributes which combine to make the  $\text{AO}^+$  state of  $\text{BiF}$  attractive as an acceptor of electronic energy from  $\text{NF}(a)$ . This process is a complex combination of energy pooling and reactive transfer which has yet to be satisfactorily elucidated. Nevertheless, the  $\text{NF}/\text{BiF}$  system is one of a small number of visible wavelength chemical laser systems currently receiving serious consideration.

There remains a considerable list of kinetic issues to be resolved. As the lower laser level of the potential lasing transition, the fate of the  $\text{BiF}(\text{XO}^+)$  is of particular concern. Evidence suggests that  $\text{BiF}$  is repetitively pumped, resulting in several  $\text{A} \rightarrow \text{X}$  photons for every  $\text{Bi}$  atom in the system. Current models of the reaction mechanism involve either the reduction of  $\text{BiF}(\text{XO}^+)$  to reform the parent  $\text{Bi}$  atom or a sequential, two-step energy transfer from  $\text{NF}(a)$ .<sup>1</sup> The principal oxidation states of bismuth are +3 and +5; both  $\text{BiF}_3$  and  $\text{BiF}_5$  are stable materials. Any process that leads to the further oxidation of  $\text{BiF}$  will remove it from the repetitive pump/lase cycle and thereby lower the overall mass efficiency of the device. We report here a study of the reactive removal of the ground state of  $\text{BiF}$  with  $\text{F}_2$  and a series of nitrogen fluorides;  $\text{NF}_2$ ,  $\text{NF}_3$ , and  $\text{N}_2\text{F}_4$ .

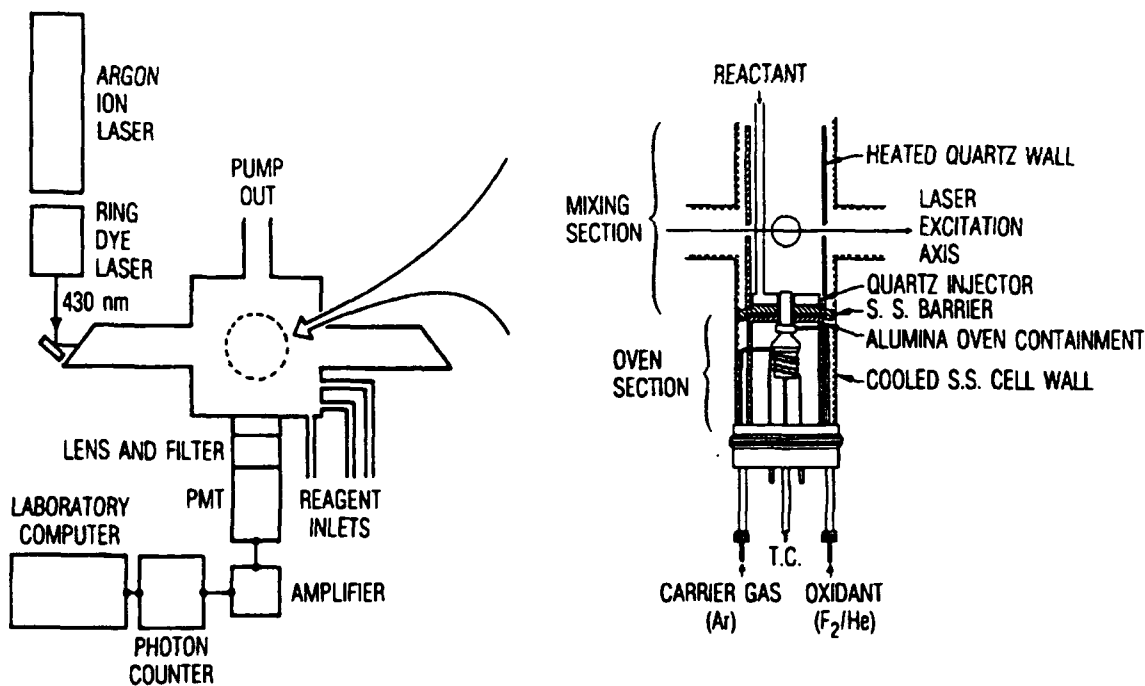
## II. EXPERIMENTAL

Two separate sets of apparatus were required to perform the BiF ground-state kinetics experiments. Steady-state measurements were made with a fixed observation point flow tube using a Broida oven<sup>5</sup> to generate a continuous flow of BiF(XO<sup>+</sup>). Because of the difficulty of accurately characterizing the various flow parameters (e.g., centerline flow velocity, see section III), these measurements were made on a relative basis. In order to obtain absolute rate coefficients, a parallel set of photolytically initiated, time-resolved experiments were conducted in a separate photolysis cell on slowly flowing, pre-mixed samples. Both experimental approaches rely on cw laser-induced fluorescence on the BiF AO<sup>+</sup>-XO<sup>+</sup> transition to monitor BiF(XO<sup>+</sup>) population. Schematic representations of both setups are shown in Figure 1.

The Broida oven/flow tube is a modification of the apparatus which we have previously employed in kinetics studies of BiF(AO<sup>+</sup>).<sup>4,6</sup> It is constructed of 4 in. nominal diameter sections of stainless steel and is operated as a flow tube in a vertical orientation. The cell is defined by two regions, the oven section and the observation region, separated by a stainless steel bulkhead. The oven consists of an alumina crucible suspended in a resistively heated tungsten basket. The crucible is filled with Bi metal. It is heated to a temperature of about 850 K, as measured by a thermocouple in contact with the outer surface of the crucible. A flow of Ar is introduced over the surface of the metal, and a stream of entrained Bi vapor is swept out of the oven section through a funnel-shaped, cylindrical stainless steel stack, 0.95 cm in diameter, which projects through the bulkhead. A dilute flow of F<sub>2</sub> (10% in He) is injected into the stack and reacts to form BiF. The crucible, tungsten filament, and gas injectors are all enclosed within an alumina housing. The stack terminates about 5 cm above the floor of the observation region as defined by the bulkhead. A quartz ring injector introduces reactant/diluent mixtures into the observation region. A quartz cylinder, 8.5 cm i.d., wrapped with nichrome wire, serves as a temperature-controlled inner wall. At the observation point, 12 cm above the end of the stack, the quartz wall is drilled through (1 cm diameter) to permit the passage of the probe laser beam. A larger port (2.5 cm diameter) is located at right angles to these holes for viewing the laser-induced fluorescence (LIF). The laser light enters and exits the cell through baffled arms equipped with Brewster-angle Suprasil windows. The LIF is collected via f/1 optics and observed through a 1.0 nm (FWHM) interference filter centered at 470.1 nm near the A-X (1,4) bandhead by a photomultiplier tube (PMT) (EMI 6256). Photon counting (Stanford Research Systems, SR400) is employed, a technique which provides a dynamic range of more than five decades. Background chemiluminescence and scattered laser light determine the sensitivity of the measurement. In all cases, this noise level is below 10<sup>3</sup> counts/sec, whereas our steady-state LIF signal levels are taken in the range of 5 x 10<sup>5</sup> - 2 x 10<sup>4</sup> counts/sec, affording the measurement excellent signal/noise ratios. The 6.5 l cell is evacuated by a 500 l/min pump. Flow rates are determined with mass flowmeters (Tylan) which were calibrated *in situ*. Total flow rates are on the order of 750 cm<sup>3</sup> atm/min.



(a) Photolysis cell.



(b) Broida oven/flow tube showing detail of oven.

Figure 1. Diagram of the Experimental Apparatus.



Pressure in the observation region of the flow tube is measured with a capacitance manometer with 10 m torr resolution (MKS Baratron). The temperature at the observation point of the flow is determined with a thermocouple located directly above the axis of the probe laser.

The photolysis cell has been described in detail previously.<sup>7</sup> Briefly, it consists of a 4.6 cm i.d. stainless steel tube 25 cm in length equipped with three orthogonal observation ports. The inner surface of the cell is Teflon coated to alleviate the effects of any wall-mediated processes. Windows on the photolysis axis are mounted on the end of 15 cm extensions to reduce scattered laser light at the observation region of the cell. The cell is wrapped with heating tape and insulated to allow operating temperatures of up to 200°C. As with the flow tube apparatus, calibrated mass flowmeters are used to measure flow rates, and cell pressure is determined with a capacitance manometer. Experiments are conducted on slowly flowing ( $< 0.25$  l-atm/min) premixed samples. In the case of the fluorine bearing reagents, mixing into the main flow is accomplished in a 0.5 in. diameter section of tubing immediately before the gas flow enters the main body of the cell. This point is of consequence to the issue of the stability of the reagents in a premixed situation. Where  $N_2F_4$  is used, it is first flowed through a quartz bulb maintained at 190°C to assure its virtually complete pyrolysis to  $NF_2$ .<sup>8,9</sup> Ground-state densities of BiF are generated via the reaction of Bi atoms with either  $NF_2$  or  $F_2$ . The Bi atoms are prepared by the ArF laser (Lambda Physik EMG 101) photolysis of trimethylbismuth,  $Bi(CH_3)_3$ , at 193 nm. Neither of the fluorine bearing reagents demonstrates an appreciable absorption at this wavelength. In order to minimize side reactions between reagents and photolysis products (chiefly  $CH_3$  fragments), the ArF laser fluence was attenuated by means of a stack of uncoated quartz flats to the lowest energy consistent with good signal-to-noise levels (3–4 mJ). BiF A–X LIF is observed through a 1.0 nm (FWHM) interference filter centered at 459.4 nm (corresponding to the A–X (1,3) bandhead) by a PMT identical to the one used on the flow tube experiments. A 25 MHz transient digitizer (LeCroy 2264) takes the time resolved data which is averaged and stored on a lab computer (DEC LSI 11/23+).

In both experiments, the BiF ground state is monitored via LIF resulting from pumping of  $v'' = 0$  using a cw ring dye laser (Coherent 699-21) with a bandwidth of about 500 kHz and single frequency powers of 150–250 mW. The pumped transition is P(24) of the A–X (1,0) band at 430.186 nm (vacuum). A wavemeter (Burleigh WA-20) is used to coarsely tune the wavelength of the laser. Fine tuning is accomplished by maximizing the BiF LIF intensity under initial experimental conditions with no reactant present. The laser frequency is actively locked to a cavity mode to ensure that there is no shift in wavelength during the experiment.

The following reagents were used without further purification: Ar (Matheson, 99.999%),  $F_2$  (Spectra Gases, 1% in Ar and 10% in He),  $SF_6$  (Alphagaz, 99.99%),  $N_2F_4$  (Hercules, 10% and 60% in Ar),  $NF_3$  (Matheson, 99.9%), and  $Bi(CH_3)_3$  (ICN Pharmaceuticals, 0.1% in Ar).

### III. RESULTS AND DISCUSSION

The rationale for following two experimental approaches in the course of this work derives from the nature of the species of interest,  $\text{BiF}(\text{XO}^+)$ , and the methodology of generating it in experimentally useful quantities. Bismuth fluoride has been observed following the photolysis of mixtures of  $\text{NF}_2$  and  $\text{Bi}(\text{CH}_3)_3$  at both 248 and 193 nm. However, production of a ground-state population of  $\text{BiF}$  in this manner presents some undesirable complications, not the least of which are the uncharacterized reactions of reagents and photolysis fragments (e.g.,  $\text{NF}_2 + \text{CH}_3$ ). As an alternative, we have used a Broida-type evaporative metal oven and subsequent oxidation to generate a continuous flow of  $\text{BiF}$ .

The use of a Broida oven entails its own complications. The primary difficulty is encountered in achieving a well characterized flow at the observation point. In order to put an amount of  $\text{Bi}$  vapor into the flow which will lead to a useful dynamic range over which to make the measurement, it is necessary to flow the  $\text{Ar}$  carrier gas at a rate that accounts for over 35% of the entire gas flow. The design of the oven is such that the  $\text{BiF}/\text{Ar}$  flow is introduced into the mixing and observation region of the apparatus through a 1 cm diameter orifice. As a result, the plug flow velocity of the entrained  $\text{BiF}$  at its point of entry into the observation region is about 30 times that calculated for the total flow in the 8 cm diameter observation region. This leads to an initially steep radial concentration gradient for  $\text{BiF}$  outside of the region defined by the central oven-flow. Further, the transport velocity<sup>10</sup>

$$v(r) = 2v_{pf}(1 - r^2/R^2), \quad (2)$$

where  $v_{pf}$  is the plug flow velocity,  $R$  is the tube radius, and  $r$  is the distance along the radius, is expected to be greater at the centerline than the  $2v_{pf}$  suggested by the total flow rate and observation region diameter. It is chiefly because of the difficulty of accurately characterizing the transport velocity that we have chosen to perform relative measurements, comparing two different reactants for a given set of flow conditions. This approach removes much of the systematic uncertainty inherent in the experiment. We then turn to a time-resolved, photolytically initiated experiment to make an absolute determination of the rate coefficient for  $\text{BiF} + \text{F}_2$ , which serves as the standard reaction to which our relative rate coefficients may be compared.

#### A. FLOW TUBE KINETIC MEASUREMENTS

OLD In order to obtain relative rates of reaction using the flow tube apparatus, the following technique is employed. A set of conditions (total flow rate, pressure, and temperature) is established which is maintained throughout the course of the experimental run. We then record  $\text{BiF}$  LIF intensity for a number of partial pressures of a particular reactant, varying the reactant/buffer gas ratio while maintaining a constant total flow rate. The result is a set of data which varies exponentially with reactant density as is expected for pseudo first-order decay;

$$[\text{BiF}] = [\text{BiF}]_0 \exp(-k_x[\text{X}]t) \quad (3)$$

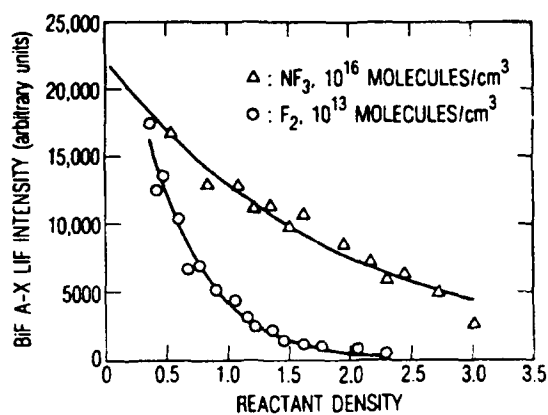
where  $k_x$  is the rate coefficient for the process of  $\text{BiF} + \text{X}$ . Two assumptions are implicit in our use of LIF as a monitor of ground-state BiF population. First, because the laser accesses a single rovibrational level of the ground state, we assume that the sample is in thermal equilibrium. The transit time to the observation point (about 16 msec), and total pressure at which the experiment is conducted (2.3 torr), ensures that the sample is vibrationally and rotationally relaxed. The second assumption is that the LIF signal intensity is proportional to the BiF ground-state population and is not affected by BiF A state kinetics. The influence of excited state kinetics is reduced due to the relatively rapid BiF(A) radiative decay. For example, an  $\text{F}_2 + \text{BiF(A)}$  removal rate constant 3 orders of magnitude larger than that for BiF(X) would only cause a 50% reduction in BiF(A) population during its 1.4  $\mu\text{sec}$  radiation lifetime<sup>4</sup> for our runs having the highest  $\text{F}_2$  densities. In the case of  $\text{NF}_2$ , the BiF A state removal rate coefficient would have to be over 4 orders of magnitude greater than BiF(X) removal for the same effect. Results from the time-resolved experiments, in which the decay of the A + X LIF intensity is strictly proportional to  $[\text{BiF(X)}]$ , are in good agreement with the flow tube study, providing further evidence that excited state kinetics do not influence the flow tube measurements.

Figure 2 displays plots of  $\text{BiF(XO}^+)$  removal by  $\text{F}_2$  and  $\text{NF}_3$  at 21°C,  $\text{F}_2$  and  $\text{N}_2\text{F}_4$  at 36°C, and  $\text{F}_2$  and  $\text{NF}_2$  at 200°C, and their least squares exponential fits. The fits to the data provide coefficients (in units of  $\text{cm}^3/\text{molecule}$ ) which represent the product  $k_x t$  where  $t$  is the transport time of the BiF from its point of injection into the mixing region of the reactor to the observation point and is taken to be constant for a given set of conditions. It will be noted that the  $\text{F}_2$  data extrapolates to a significantly larger intercept than does its partner in each of the three data sets. The reactants employed in these experiments are capable of both the initial oxidation of Bi atoms to form BiF and further reaction to remove it. Because the experiment is constrained to a single fixed observation point and reaction distance, it is not possible to uniquely resolve formation and removal processes. Care is taken that the  $\text{F}_2$  injected into the entrained Bi stream in the oven section to form BiF is present in sufficient excess so that no unreacted Bi remains. The  $\text{F}_2$  data suggest that some further BiF formation does take place at low reactant densities. In the regime in which the data is taken, however, the decay of the signal is single exponential with reactant density. We take this as indicative that the process we are following is completely dominated by the removal of BiF, with no contribution due to its formation. The agreement of these results with the photolytic experiments bears this assumption out.

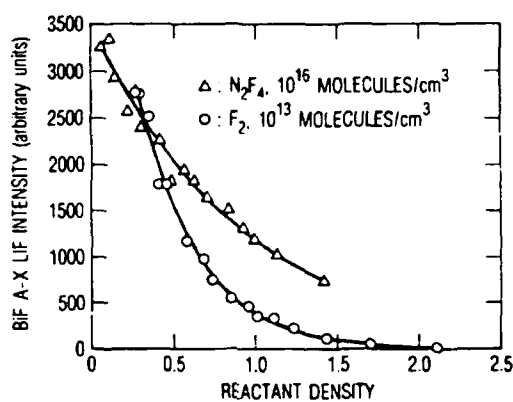
The experimental sets are always performed as pairs, with one reaction treated as the standard against which the others are compared. We have chosen the rate of



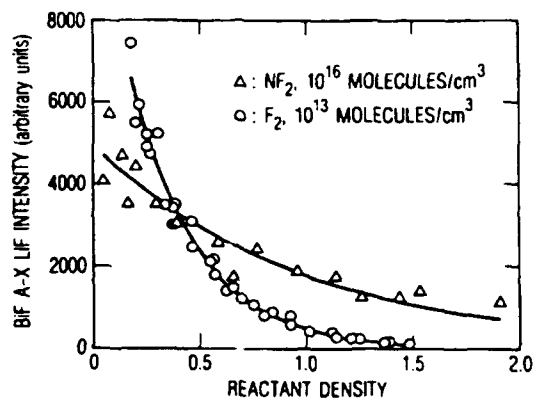
as the standard rate for these measurements. Table 1 summarizes the results of the flow tube determinations for  $\text{NF}_2$ ,  $\text{N}_2\text{F}_4$ , and  $\text{NF}_3$ , as well as the absolute rate coefficients obtained from our time-resolved measurements. Error limits quoted are the rms errors



(a) Data for  $\text{NF}_3$  and  $\text{F}_2$  at  $21^\circ\text{C}$



(b) Data for  $\text{N}_2\text{F}_4$  and  $\text{F}_2$  at  $36^\circ\text{C}$



(c) Data for  $\text{NF}_2$  and  $\text{F}_2$  at  $200^\circ\text{C}$

Figure 2. BiF A-X Laser-Induced Fluorescence Intensity Plotted as a Function of Reactant Density.  $\text{F}_2$  density is represented by circles and reactant density by triangles. Solid lines are least squares single exponential fits to the data.

Table 1. Results of BiF + X

X	Method	Temperature (K)	$k_x/k_{F_2}$	$k_x(\text{cm}^3/\text{molecule-sec})$
F <sub>2</sub>	Time Resolved	298		$2.1 (0.2) \times 10^{-11}$
F <sub>2</sub>	Time Resolved	463		$2.0 (0.2) \times 10^{-11}$
NF <sub>2</sub>	Flow Tube	473	$3.08 \times 10^{-4}$	$6.2 (2.2) \times 10^{-15}$
NF <sub>2</sub>	Time Resolved	471		$3.9 (1.0) \times 10^{-15}$
NF <sub>3</sub>	Flow Tube	294	$2.51 \times 10^{-4}$	$5.0 (1.4) \times 10^{-15}$
N <sub>2</sub> F <sub>4</sub>	Flow Tube	309	$3.91 \times 10^{-4}$	$7.8 (1.6) \times 10^{-15}$
BiF Formation				
Bi + NF <sub>2</sub>	Time Resolved	468		$8.1 (1.9) \times 10^{-12}$
Bi + F <sub>2</sub>	Time Resolved	298		$\sim 1 \times 10^{-9}$

based on  $2\sigma$  from the nonlinear least squares fits to the data. The flow tube experiments provide us with relative rate coefficients,  $k_x/k_{F_2}$ . We require an absolute value for  $k_{F_2}$ .

Performing our kinetic measurements in a relative fashion presents a number of advantages. Because we duplicate flow tube conditions for each of the reactants for a given experimental run, we obtain relative rate coefficients which are independent of the uncertainties associated with the flow dynamics. The principal deviation from this assumption arises from the difference in the diffusivities of the various reactants, in so far as mixing of the reactants into the BiF flow is incomplete. Given the distance from the reactant injector to the observation point (15 cm) and reactor pressure (2.3 Torr), this effect is negligible. Reactant concentrations are varied such that the same range of steady-state intensities is observed in each case. As a result, any contribution from axial diffusion to the overall transport velocity will be the same for each set of measurements.

Analysis of the removal of BiF by N<sub>2</sub>F<sub>4</sub> at 300°C requires that the equilibrium concentration of NF<sub>2</sub> be accounted for. At this temperature, NF<sub>2</sub> is present at levels of 10 to 50% that of N<sub>2</sub>F<sub>4</sub> depending on the overall partial pressure of two species.<sup>8,9</sup> The observed rate of removal of BiF is simply the sum of the products of the reactant densities and their associated rate coefficients.

$$R_{obs} = (k_{N_2F_4} [N_2F_4] + k_{NF_2} [NF_2]) \quad (5)$$

The BiF density at the observation point is

$$[BiF] = [BiF]_0 \exp\{-(k_{N_2F_4} [N_2F_4] + k_{NF_2} [NF_2])t\} \quad (6)$$

To extract the ratio  $k_{N_2F_4}/k_{F_2}$  from the flow tube intensity data, each experimental point is scaled according to the previously obtained rate coefficient for NF<sub>2</sub> at 200°C, the partial

pressure of  $\text{NF}_2$  for that measurement, and the transport time,  $t$ . The transport time is calculated on the basis of comparison of the corresponding  $\text{F}_2$  data with the results of our time resolved measurements. No correction is made for any temperature dependence of the  $\text{NF}_2$  rate coefficient. The rate coefficients for the monomer and dimer are similar enough that, when no correction is made for the partial pressure of  $\text{NF}_2$ , a coefficient of  $8.9 \times 10^{-15}$  is obtained, well within the error of the value we quote for  $k_{\text{N}_2\text{F}_4}$ .

A summary of bond dissociation energies derived from available thermochemical data for bismuth and nitrogen fluorides is presented in Table 2. Although the  $\text{BiF-F}$  and  $\text{BiF}_2\text{-F}$  bond energies for  $\text{BiF}_2$  and  $\text{BiF}_3$  are not known, the average bond energy of  $\text{BiF}_3$  is 91.1 kcal/mol.<sup>11</sup> Estimates of the bond strength of  $\text{BiF}(\text{XO}^+)$ , based on spectroscopic evidence, range from 74 kcal/mol<sup>3,12</sup> to 115 kcal/mol on the basis of a LeRoy-Bernstein long-range analysis of the  $\text{BiF}(\text{XO}^+)$  state in recent work by Ross, et al.<sup>13</sup> The N-F bond energy increases with decreasing degree of fluorination ranging from 59.3 kcal/mol for  $\text{NF}_2\text{-F}$  to 71.7 kcal/mol for  $\text{NF}(\text{X})$ . Also included in the table are the  $\text{NF}(\text{a})$  and  $\text{NF}(\text{b})$  dissociation energies, calculated using NF spectroscopic data.<sup>15,16</sup> Assuming a release of 90 kcal/mol for the formation of the second  $\text{BiF-F}$  bond, the fluorination of  $\text{BiF}(\text{XO}^+)$  by  $\text{NF}_2$  and  $\text{F}_2$  will be exothermic by 23 kcal/mol and 53 kcal/mol, respectively.

Table 2. Bismuth and Nitrogen Fluoride Bond Dissociation Energies

SPECIES	Dissociation Energy		Reference
	( $\text{cm}^{-1}$ )	kcal/mole	
$\text{F}_2$	12920(50)	36.93(0.10)	14
$\text{NF}(\text{b})^{(\text{a})}$	25100(2800)	71.5(7.9)	16
$\text{NF}(\text{a})^{(\text{a})}$	32600(2800)	93.2(7.9)	15
$\text{NF}(\text{X})$	25000(2800)	71.7(7.9)	14
$\text{NF-F}$	23500(2800)	67.2(7.9)	14
$\text{NF}_2\text{-F}$	20700(700)	59.3(1.9)	14
$\text{BiF}$	25800	74	3,12
$\text{BiF}^{(\text{b})}$	31900(590)	91.1(1.7)	11
$\text{BiF}$	40000	115	13

<sup>(a)</sup>Calculated using the  $\text{NF}(\text{X})$  bond energy and spectroscopic data, where the dissociated atoms are assumed to be  $\text{N}(^2\text{D})$  and  $\text{F}(^2\text{P})$ .

<sup>(b)</sup>Average bond strength from the enthalpy of atomization.

The rate coefficients which we report for the different nitrogen fluorides are statistically the same. Essentially the same processes of bond formation and cleavage are being undergone in each instance with the same thermochemistry dominating the reaction. From the point of view of a simple Arrhenius interpretation, there is apparently not a strong temperature dependence for the reaction. However, the estimated error in the rate coeffi-

cients we report is sufficiently large to disguise an activation barrier of up to about 1 kcal/mol. Zero or negative temperature dependencies are often attributed to the formation of bound intermediates<sup>17</sup> where the observed rate reflects the equilibria of the transition complex with both the starting material and the products. Alternatively, steric differences among the various reactants may serve to counter the effect of temperature on the rates which we observe. An explicit investigation of the rate of the reaction as a function of temperature is necessary before any conclusions may be drawn concerning the microscopic detail of the process. The use of  $\text{NF}_3$  as the test case would provide a system that is stable over a wide range of temperatures with the salient features of  $\text{NF}_2/\text{N}_2\text{F}_4$ , in particular the 60–70 kcal/mol N–F bond and the lone pair of electrons on the central N atom.

## B. PHOTO-INITIATED KINETICS

Once the relative rates of reaction have been established, an absolute rate coefficient must be determined for our baseline reaction,  $\text{BiF} + \text{F}_2$ . To this end we have performed a time-resolved experiment based on ArF laser photolysis of  $\text{Bi}(\text{CH}_3)_3$  at 193 nm and the subsequent formation and removal of BiF by  $\text{F}_2$ . Measurements were performed at 20 and 190°C. As a check of our flow tube results, we have measured the rate of removal of BiF with  $\text{NF}_2$  at 190°C. We have also determined the rate of formation of BiF from  $\text{Bi} + \text{NF}_2$ . We conclude with some observations on stability of these reagents with regard to one another in so far as it affects the ability to premix these compounds.

In order to minimize the effect of undesired side reactions on our measurement, both the ArF photolysis laser flux and the initial  $\text{Bi}(\text{CH}_3)_3$  density were held to relatively low values (3 mJ and  $2\text{--}3 \times 10^{12}$  molecules/cm<sup>3</sup>, respectively). Experimental conditions were chosen where  $[\text{F}_2] > 10[\text{Bi}(\text{CH}_3)_3]$  so that loss of  $\text{F}_2$  due to the generation of BiF and any side reactions would be insignificant. Our method is simple. Fluorine reacts rapidly with the Bi atoms generated by the 193-nm photolysis of  $\text{Bi}(\text{CH}_3)_3$  to form BiF. On the timescale of the subsequent decay of the BiF LIF signal, the resultant time-resolved traces are well represented by a single exponential decay. Figure 3 provides an example of the signal and its nonlinear least squares fit. Fits of this data provide rates of removal which are in turn plotted against the  $\text{F}_2$  density at which the data were taken, as in Figure 4. The slope of the linear least squares fit to the rate vs density data yields the rate coefficient for the process. Care was taken to ensure that the rates we measure are a function only of  $\text{F}_2$  density and do not include contributions from relaxation of a nascent product distribution or unwanted side reactions.  $\text{SF}_6$  is employed as a constituent of the buffer gas mixture to promote the rapid vibrational relaxation of the reaction products. Previous work<sup>7</sup> has shown  $\text{SF}_6$  to be an efficient vibrational quencher of  $\text{BiF}(\text{A})$ . Variations in the partial pressure of  $\text{SF}_6$  have no effect on the measured rate of decay of the LIF signal. Similarly, the observed rates are invariant to excursions in  $\text{Bi}(\text{CH}_3)_3$  density. The cluster of eight points in Fig. 4 confirms that the decay rates are dependent only on  $\text{F}_2$ . The rate coefficient determined for  $\text{BiF} + \text{F}_2$ ,  $2.0 \times 10^{-11}$  cm<sup>3</sup>/molecule-sec, forms the basis for the analysis of the flow tube measurements. The rate coefficient determined for  $\text{BiF} + \text{F}_2$ ,  $2.0 \times 10^{-11}$  cm<sup>3</sup>/molecule-sec, forms the basis for the analysis of the flow tube measurements.

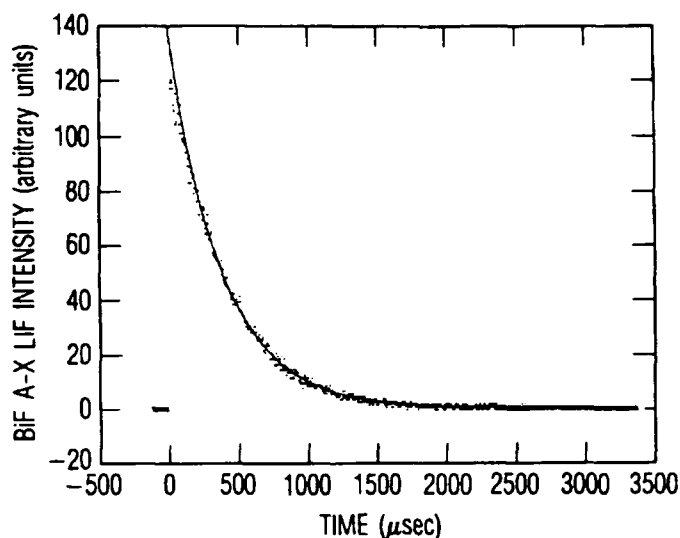


Figure 3. Time-resolved BiF A-X Laser-Induced Fluorescence from the 193 nm Photolysis of a Mixture of  $F_2$  ( $1.37 \times 10^{14}$  molecules/ $cm^3$ ), Ar ( $1.87 \times 10^{17}$  atoms/ $cm^3$ ),  $SF_6$  ( $7.55 \times 10^{16}$  molecules/ $cm^3$ ), and  $Bi(CH_3)_3$  ( $7.76 \times 10^{12}$  molecules/ $cm^3$ ) at  $25^\circ C$ . The solid line is a least squares single exponential fit to the data.

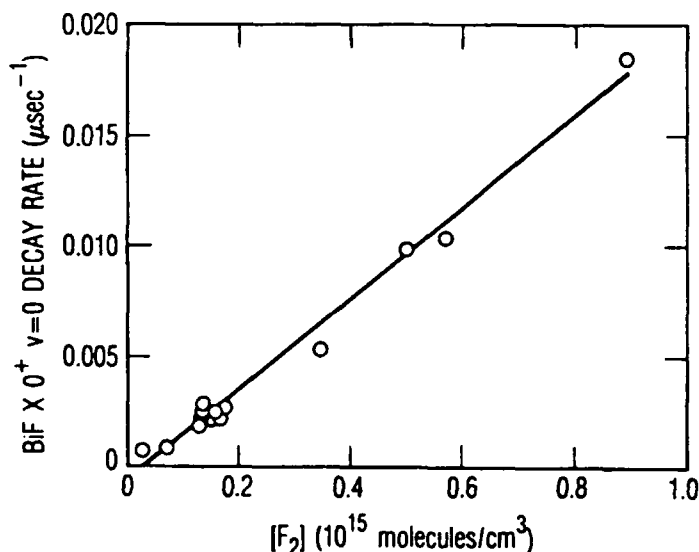


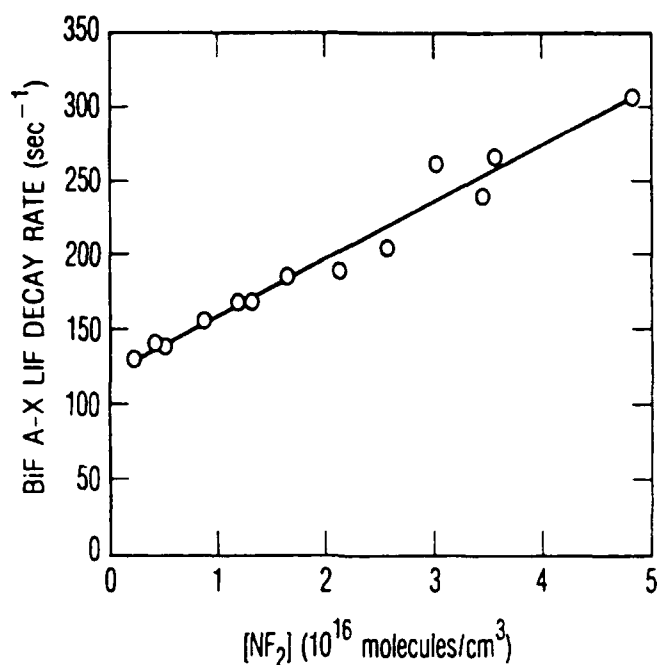
Figure 4. Plot of BiF A-X Laser-Induced Fluorescence Decay Rates from the 193 nm Photolysis of  $F_2/Ar/SF_6/Bi(CH_3)_3$  Mixtures at  $25^\circ C$ . The solid line is a linear fit to the data and has a slope of  $2.1 \pm 0.3 \times 10^{-11}$   $cm^3/molecule\cdot sec$ . The cluster of data points near  $[F_2] = 1.5 \times 10^{14}$ , which is the result of variations in the partial pressures of  $SF_6$  and  $Bi(CH_3)_3$ , demonstrates that the rate is solely a function of  $F_2$  density.



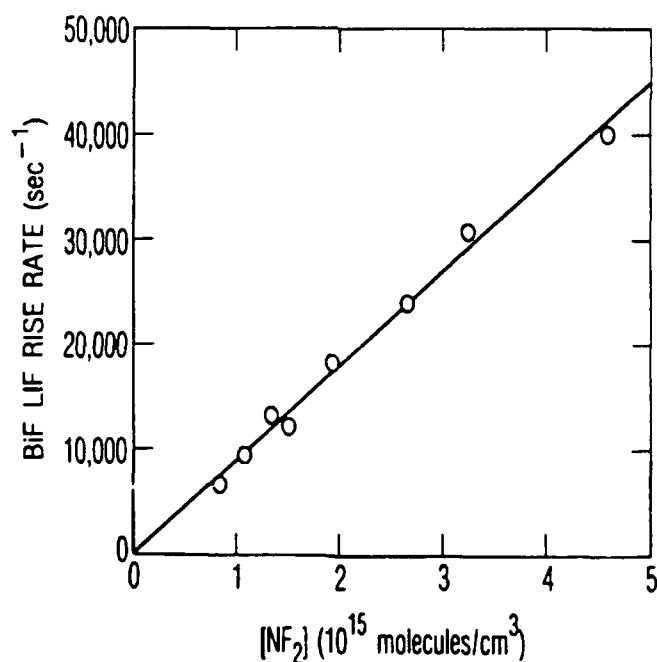
Similar experiments were performed with  $\text{NF}_2$  as the oxidant. The use of low photolysis energy and small  $\text{Bi}(\text{CH}_3)_3$  concentrations was especially necessary in these instances. Where higher fluences and  $\text{Bi}(\text{CH}_3)_3$  densities were employed, the resulting LIF signals could only be fit to double exponential decays. We take this as indicative of reaction of  $\text{NF}_2$  with photolysis fragments. Figure 5 displays a decay rate vs density plot for  $\text{NF}_2$ . The rate coefficient which we obtain for  $\text{BiF} + \text{NF}_2$  from our time resolved measurements,  $3.9 \times 10^{-15} \text{ cm}^3/\text{molecule-sec}$ , compares reasonably well with the results of the flow tube work. The two values are within about 40% of one another and agree within their limits of error. We prefer the later value despite its somewhat larger error bars. Although photolytically initiated experiments are necessary to analyze the results, the Broida oven/flow tube measurements are performed on a system which is largely free of complications arising from the presence of uncharacterized side reactions.

It was observed that the risetime of the  $\text{BiF}$  LIF signal from  $\text{Bi} + \text{NF}_2$  was resolvable within our experimental bandwidth. A plot of the rate of formation of  $\text{BiF}$  vs  $\text{NF}_2$  density is also shown in Figure 5. The rate coefficient for the formation of  $\text{BiF}(\text{XO}^+)$  from  $\text{Bi} + \text{NF}_2$  is also reported in Table I. The  $\text{BiF}$  risetime from  $\text{Bi} + \text{F}_2$  was too rapid to be resolved at high  $\text{F}_2$  densities, and at low  $\text{F}_2$  densities the signal-to-noise ratio suffered due to the reaction of  $\text{F}_2$  with  $\text{Bi}(\text{CH}_3)_3$ . Although we were not able to achieve satisfactory results, attempts to determine the  $\text{BiF}$  formation rate indicate that the reaction is extremely fast, on the order of  $1 \times 10^{-9} \text{ cm}^3/\text{molecule-sec}$ . It must be noted that there is a wide disposition in the energy levels of  $\text{Bi}$  atoms produced by the 193-nm photolysis of  $\text{Bi}(\text{CH}_3)_3$ .<sup>7</sup> In particular, the upper lying spin-orbit states of the  $6p^3$  ground-state configuration are optically metastable and may be expected to participate in the reaction to form  $\text{BiF}$ . Therefore, the measurement is made over an ensemble of energy states of the  $\text{Bi}$  atom. The value of  $8.1 \times 10^{-12} \text{ cm}^3/\text{molecule-sec}$  is within reasonable agreement with unpublished results from our laboratory of the rate coefficient for the removal of  $\text{Bi}(^2\text{D}_{3/2})$  by  $\text{NF}_2$  of  $\leq 1.2(0.3) \times 10^{-11}$ . Whereas the latter value is specific with regard to the collision partners, the formation constant must be viewed as a weighted average over the various states of  $\text{Bi}$  present; primarily the  $^4\text{S}_{3/2}$  ground state and the first excited  $^2\text{D}_{3/2}$  spin-orbit state. As such, the agreement between the two measurements is rather good and, unless the  $\text{Bi}(^4\text{S}_{3/2})$  and  $\text{Bi}(^2\text{D}_{3/2})$  rate constants are similar, these results suggest that the  $\text{Bi}(^2\text{D}_{3/2})$  state dominates either the reaction or the photolytic population distribution at early times.

The formation of  $\text{BiF}$  in the photolytic experiments is complex. A significant amount of energy is present in the form of electronic excitation of the  $\text{Bi}$  atoms. The term energy of  $\text{Bi}(^2\text{D}_{3/2})$  is  $11419 \text{ cm}^{-1}$  (32.6 kcal/mol).<sup>19</sup> In addition, the products possess a number of low-lying electronic states. Assuming a bond energy of 90 kcal/mol for  $\text{BiF}$ , the  $\text{NF}_2 + \text{Bi}(^2\text{D}_{3/2})$  reaction can liberate as much as 55 kcal/mol, and 23 kcal/mol is available from the  $\text{NF}_2 + \text{Bi}(^4\text{S}_{3/2})$  reaction.<sup>16,17,20</sup> Thus, a large number of exothermic channels are possible.

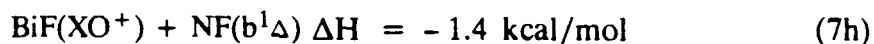
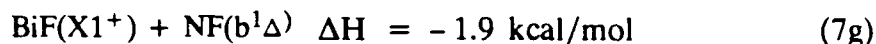
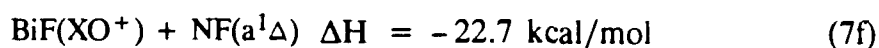
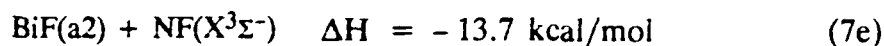
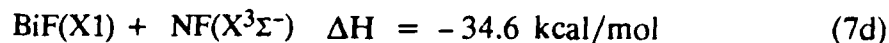
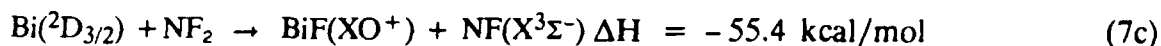
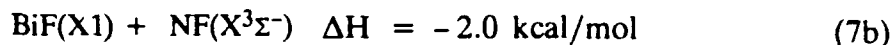
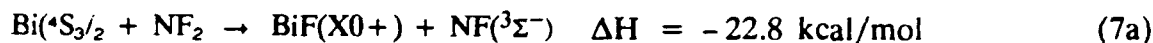


(a) BiF A-X LIF Decay Rate vs NF<sub>2</sub> Density. Solid line is a linear fit to the data with a slope of  $3.9 \pm 0.5 \times 10^{-15} \text{ cm}^3/\text{molecule-sec}$ .



(b) BiF A-X LIF Rise Rate vs NF<sub>2</sub> Density. Solid line is a linear fit to the data with a slope of  $9.0 \pm 1.0 \times 10^{-12} \text{ cm}^3/\text{molecule-sec}$ .

Figure 5. Plots of BiF A-X Laser-Induced Fluorescence Decay and Rise Rates from ArF Laser Initiation of NF<sub>2</sub>/Ar/SF<sub>6</sub>/Bi(CH<sub>3</sub>)<sub>3</sub> Mixtures at 198°C.



The formation of charge-transfer complex intermediates has been suggested in the reaction of alkali metal atoms with halogen molecules.<sup>18</sup> In a somewhat different context, a simplified long range attractive potential model has been applied to the formation of  $\text{Bi}(^2\text{D}_{3/2})$  from  $\text{Bi} + \text{NF}(\text{a}^1\Delta)$  (Reaction 1).<sup>19</sup> The model proposes a curve crossing from the covalent  $\text{M} + \text{X}_2$  surface to the charge-transfer complex potential surface for  $\text{M}^+ + \text{X}_2^-$ . The crossing occurs at a separation  $R_0$  determined by the potential energy of the neutral collision pair, given at large  $R$  by

$$U(R_0) = \text{IP}(\text{M}) - \text{EA}(\text{X}_2) \quad (8)$$

where  $\text{IP}(\text{M})$  is the ionization potential of the metal atom and  $\text{EA}(\text{X}_2)$  is the electron affinity of the halogen. The potential of the ion pair may be approximated by coulombic and charge-induced dipole terms:

$$U(R) = -e^2/R - e^2(\alpha^+ + \alpha^-)/2R^4 \quad (9)$$

where  $e$  is the unit of elementary charge and  $\alpha^+$  and  $\alpha^-$  are the polarizabilities of the ion pair. For the present case of  $\text{Bi} + \text{F}_2$ , we take  $\text{IP}(\text{Bi } ^4\text{S}, ^2\text{D}) = 7.28, 5.86 \text{ eV}$ ,<sup>20</sup> and  $\text{EA}(\text{F}_2) = 3.08 \text{ eV}$ .<sup>21</sup> The polarizability of  $\text{Bi}^+$  is estimated using Slater's rules,<sup>22</sup>  $\alpha^+ = 2.96 \times 10^{-23} \text{ cm}^3$ . We take the polarizability of  $\text{F}_2^-$ , to be somewhat greater than that of  $\text{O}_2$ ,  $\alpha^- = 2.4 \times 10^{-24} \text{ cm}^3$ .<sup>22</sup> Equating the two potentials yields reactive cross sections of 64 and 113 Å for  $\text{Bi}(^4\text{S})$  and  $\text{Bi}(^2\text{D}) + \text{F}_2$ , respectively.<sup>2</sup> The cross sections in turn correspond to rate coefficients of  $3.5$  and  $6.3 \times 10^{-10} \text{ cm}^3/\text{molecule-sec}$ . Considering the conceptual simplicity of the model, agreement with the experiment is quite good. The results also lend some credence to our earlier supposition that  $\text{Bi}(^2\text{D}_{3/2})$  is the major reactive species in the photolytically initiated environment.

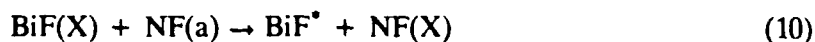
Bell and Husain<sup>23</sup> have measured the removal of  $\text{Bi}(^4\text{S})$  with  $\text{Br}_2$ . The rate constant they report,  $5.3 \times 10^{-13} \text{ cm}^3/\text{molecule-sec}$ , suggests that a different mechanism is operative.

The primary differences of that system in comparison to the present case are to be found in the electron affinity of  $\text{Br}_2$  (2.5 eV)<sup>21</sup> and the restriction of the measurement to ground-state Bi. Both these considerations have the effect of lowering the long range covalent potential by about 2 eV relative to  $\text{Bi}(^2\text{D}) + \text{F}_2$ . This results in the prediction of an equipotential separation of somewhat less than 4 Å, which is well within the covalent hard-sphere collision diameter for  $\text{Bi} + \text{Br}_2$ .<sup>22,24</sup> Thus, for a crossing to occur, it would necessarily have to take place on a repulsive slope of the potential surface of the reaction.

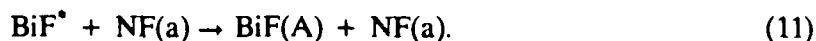
Trainor<sup>25</sup> has measured the rate of reaction of  $\text{Bi}(^2\text{D}) + \text{O}_2$  over a range of temperatures. His reported rate coefficients ( $0.37 - 1.2 \times 10^{-12}$  cm<sup>3</sup>/molecule-sec,  $T = 300 - 450$  K) suggest that the reaction proceeds under the influence of the thermodynamic barrier rather than by means of a long range attractive potential. The electron affinity of  $\text{O}_2$ , 0.44 eV,<sup>26</sup> is less than half that of the Bi atom (0.946 eV).<sup>27</sup> There is no propensity for an electron jump to take place.

During the course of the experiments described here, it was noticed that the initial BiF LIF intensities declined with increasing  $\text{NF}_2$ . We investigated this effect by simultaneously interrupting the reagent flows and sealing the flow cell. We monitored  $\text{Bi}(\text{CH}_3)_3$  in absorption using the output of a deuterium lamp restricted by an interference filter at 206 nm and detected with a monochromator and PMT. At 211°C, with no  $\text{NF}_2$  present, the  $\text{Bi}(\text{CH}_3)_3$  displayed a characteristic lifetime in the photolysis cell of almost 200 sec before presumably being decomposed on the walls. This characteristic time increased by nearly a factor of 10 at 20°C, although the effect is complicated somewhat by fairly rapid ( $0.02 \text{ sec}^{-1}$ ) initial decay which we take to be adsorption on the cell walls. However, the addition of  $\text{NF}_2$  at elevated temperature removes  $\text{Bi}(\text{CH}_3)_3$  with a rate constant of  $2 \times 10^{-18}$  cm<sup>3</sup>/molecule-sec. Figure 6 displays our measured disappearance rates as a function of  $\text{NF}_2$  density at 205°C. This process is of no consequence to the present study, but must be considered in such instances where Bi atom densities must be scaled via the UV photolysis of  $\text{Bi}(\text{CH}_3)_3$ .

The slow pace at which the N-F bond is converted to Bi-F in the removal of BiF is of positive import for the NF(a)-driven BiF chemical laser system. The pumping of  $\text{BiF}(\text{AO}^+)$  by NF(a) is thought to proceed via an intermediate BiF electronic state in a two-step mechanism,



followed by



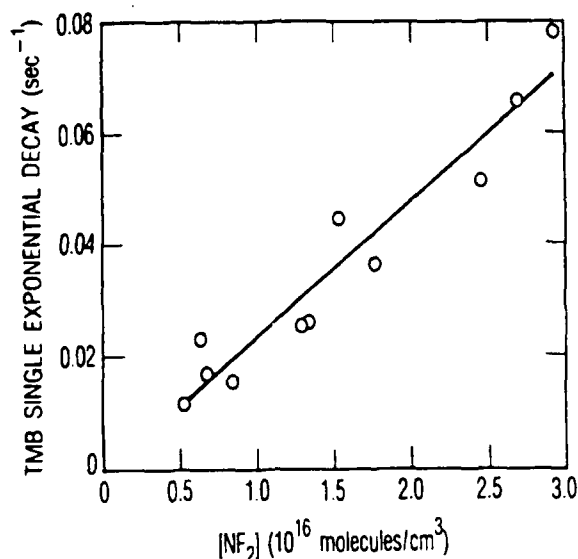


Figure 6. Plot of  $\text{Bi}(\text{CH}_3)_3$  Single Exponential Removal Rates by its Reaction with  $\text{NF}_2$  at  $205^\circ\text{C}$ . Solid line has a slope of  $2.4 \pm 1.5 \times 10^{-18} \text{ cm}^3/\text{molecule-sec}$ .

Rate constants for each step are estimated to be of the order of  $10^{-10}$  to  $10^{-11} \text{ cm}^3/\text{molecule-sec}$ ,<sup>28,29</sup> several orders of magnitude larger than the  $\text{NF}_2 + \text{BiF}(\text{X})$  rate coefficient reported here. Thus removal of  $\text{BiF}(\text{X})$  due to reaction with  $\text{NF}_2$  will not compete effectively with  $\text{NF}(\text{a})$  pumping in such systems where  $[\text{NF}(\text{a})] \gg [\text{NF}_2]$ . While  $\text{F}_2$  has proven to remove  $\text{BiF}$  efficiently, it does not exist in substantial density in the laser medium.

## VI. CONCLUSION

We have measured the rate of removal of BiF in its ground electronic state with a series of fluorine atom donors. The kinetics were determined using both flow tube and time-resolved techniques. Both methods yield consistent results. While F<sub>2</sub> is found to be relatively fast, the series of nitrogen fluorides, NF<sub>2</sub>, NF<sub>3</sub>, and N<sub>2</sub>F<sub>4</sub>, are all quite inefficient.

## REFERENCES

1. J. M. Herbelin and R. A. Klingberg, *Int. J. Chem. Kinet.* **16**, 849 (1984).
2. G. A. Capelle, D. G. Sutton and J. I. Steinfeld, *J. Chem. Phys.* **69**, 5140 (1978).
3. W. E. Jones and T. D. McLean, *J. Mol. Spectrosc.* **90**, 481 (1981).
4. R. F. Heidner, H. Helvajian, J. S. Holloway, and J. B. Koffend, *J. Chem. Phys.* **84**, 2137 (1986).
5. C. R. Jones and H. P. Broida, *J. Chem. Phys.* **60**, 4369 (1974).
6. H. Helvajian, J. S. Holloway, and J. B. Koffend, *J. Chem. Phys.* **89**, 4450 (1988).
7. J. S. Holloway, J. B. Koffend, R. F. Heidner, *J. Phys. Chem.* **93**, 7665 (1989).
8. S. N. Foner, and R. L. Hudson, *J. Chem. Phys.* **58**, 581 (1973).
9. P. J. Evans and E. J. Tschuikow-Roux, *J. Phys. Chem.* **82**, 182 (1978).
10. C. J. Howard, *J. Phys. Chem.* **83**, 3 (1979).
11. D. Cubicciotti *J. Electrochem. Soc.* **115**, 1138 (1968).
12. B. Rai and J. Singh, *Spectrosc. Lett.* **4**, 129 (1971).
13. A. J. Ross, R. Bacis, J. d'Incan, C. Effantin, J. B. Koffend, A. Toupouzkhian, and J. Verges, *Chem. Phys. Lett.* **166**, 539 (1990).
14. JANAF Tables Of Thermochemical Data, *J. Phys. Chem. Ref. Data*, Vol. 14, suppl. 1 (1985).
15. W.E. Jones, *Can. J. Phys.* **45**, 21 (1967).
16. M. Vervloet and J.K.G. Watson, *Can. J. Phys.* **64**, 1529 (1986).
17. A. Fontijn and R. Zellner, "Influence of Temperature on Rate Coefficients of Bimolecular Reactions" in *Reactions of Small Transient Species*, A. Fontijn and M. A. A. Clyne Eds., Academic Press, London (1983).
18. E. A. Gislason and J. G. Sachs, *J. Chem. Phys.* **62**, 2678 (1975) and references therein.
19. J. I. Steinfeld and D. G. Sutton, *Chem. Phys. Lett.* **64**, 550 (1979).
20. C. E. Moore, Ed., *Atomic Energy Levels*, Natl. Bur. Stand. Circ. No. 467 (1958).
21. W. A. Chupka, J. Berkowitz, and D. Gutman, *J. Chem. Phys.* **55**, 2724 (1971).
22. J. O. Hirschfelder, C. F. Curtis, and R. B. Bird, *Molecular Theory of Gases and Liquids*, John Wiley and Sons, Inc., New York, (1964).
23. C. F. Bell and D. Husain, *J. Photochem.* **26**, 229 (1984).
24. J. C. Slater, *J. Chem. Phys.* **41**, 3199 (1964).
25. D. W. Trainor, *J. Chem. Phys.* **67**, 1206 (1977).

26. R. J. Celotta, R. A. Bennet, J. L. Hall, M. W. Siegel, and J. Levine, Phys. Rev. **A6**, 631 (1972).
27. H. Hotop and W. C. Lineberger, J. Phys. Chem. Ref. Data **4**, 539 (1985).
28. J.M. Herbelin, Conf. Proc., Intl. Conf. on Lasers '86, 218 (1986).
29. J.M. Herbelin, Conf. Proc., Intl. Conf. on Lasers '87, 281 (1987).



## LABORATORY OPERATIONS

The Aerospace Corporation functions as an "architect-engineer" for national security projects, specializing in advanced military space systems. Providing research support, the corporation's Laboratory Operations conducts experimental and theoretical investigations that focus on the application of scientific and technical advances to such systems. Vital to the success of these investigations is the technical staff's wide-ranging expertise and its ability to stay current with new developments. This expertise is enhanced by a research program aimed at dealing with the many problems associated with rapidly evolving space systems. Contributing their capabilities to the research effort are these individual laboratories:

**Aerophysics Laboratory:** Launch vehicle and reentry fluid mechanics, heat transfer and flight dynamics; chemical and electric propulsion, propellant chemistry, chemical dynamics, environmental chemistry, trace detection; spacecraft structural mechanics, contamination, thermal and structural control; high temperature thermomechanics, gas kinetics and radiation; cw and pulsed chemical and excimer laser development, including chemical kinetics, spectroscopy, optical resonators, beam control, atmospheric propagation, laser effects and countermeasures.

**Chemistry and Physics Laboratory:** Atmospheric chemical reactions, atmospheric optics, light scattering, state-specific chemical reactions and radiative signatures of missile plumes, sensor out-of-field-of-view rejection, applied laser spectroscopy, laser chemistry, laser optoelectronics, solar cell physics, battery electrochemistry, space vacuum and radiation effects on materials, lubrication and surface phenomena, thermionic emission, photosensitive materials and detectors, atomic frequency standards, and environmental chemistry.

**Electronics Research Laboratory:** Microelectronics, solid-state device physics, compound semiconductors, radiation hardening; electro-optics, quantum electronics, solid-state lasers, optical propagation and communications; microwave semiconductor devices, microwave/millimeter wave measurements, diagnostics and radiometry, microwave/millimeter wave thermionic devices; atomic time and frequency standards; antennas, rf systems, electromagnetic propagation phenomena, space communication systems.

**Materials Sciences Laboratory:** Development of new materials: metals, alloys, ceramics, polymers and their composites, and new forms of carbon; nondestructive evaluation, component failure analysis and reliability; fracture mechanics and stress corrosion; analysis and evaluation of materials at cryogenic and elevated temperatures as well as in space and enemy-induced environments.

**Space Sciences Laboratory:** Magnetospheric, auroral and cosmic ray physics, wave-particle interactions, magnetospheric plasma waves; atmospheric and ionospheric physics, density and composition of the upper atmosphere, remote sensing using atmospheric radiation; solar physics, infrared astronomy, infrared signature analysis; effects of solar activity, magnetic storms and nuclear explosions on the earth's atmosphere, ionosphere and magnetosphere; effects of electromagnetic and particulate radiations on space systems; space instrumentation.